Malaysian Journal of Chemical Engineering & Technology 6(2) (2023) 81–87

Malaysian Journal of Chemical Engineering & Technology

Journal Homepage: http://myjms.mohe.gov.my/index.php/mjcet

e-ISSN: 2682-8588

Morphological, structural and optical properties of ZnO nanowires: The effect of growth time

[a,b] Nurul Zulaikha Mohd Zamri, [a,b] Mohd Firdaus Malek*, [a,b,c] Maryam Mohammad, [a,b] Mohd Dzulfiqar Bakri, [a,b] Nur Fairuz Rostan, [a,b] Nurfatini Atiqrah Khairul Azhar, [d] Mohamad Hafiz Mamat, [e,f] Muhammad Salleh Shamsudin, [a,d] Mohamad Rusop Mahmood

[a]NANO-SciTech Lab (NST), Centre for Functional Materials and Nanotechnology (FMN), Institute of Science (IOS), Universiti Teknologi MARA (UiTM), 40450 Shah Alam, Selangor, Malaysia

[b]Faculty of Applied Sciences, Universiti Teknologi MARA (UiTM), 40450 Shah Alam, Selangor, Malaysia

[c]Department of, Faculty of Applied Sciences, Universiti Teknologi MARA (UiTM), Perak Branch, Tapah Campus, Tapah Road, 35400 Perak, Malaysia

[d]NANO-ElecTronic Centre (NET), Faculty of Electrical Engineering, Universiti Teknologi MARA (UiTM), 40450 Shah Alam, Selangor, Malaysia

[e]Smart Manufacturing and Systems Research Group (SMSRG), University of Southampton Malaysia (UoSM), 79100 Iskandar Puteri, Johor, Malaysia

[f]Laser Centre, Ibnu Sina Institute for Scientific and Industrial Research, Universiti Teknologi Malaysia (UTM), 81310 Skudai, Johor, Malaysia

*Corresponding email: mfmalek07@uitm.edu.my; mfmalek07@gmail.com

Abstract

Zinc oxide (ZnO) nanostructures (NSs) such as nanowires (NWs), nanorods, nanobelts, nanotubes, and nanonails have received a lot of attention in recent years due to their exceptional chemical and physical characteristics and wide range of potential uses. Researchers have investigated its possible uses in optoelectronic devices, field emitters, solar cells, sensors, and transparent electrodes due to its special features. This work is focused on a new method for the synthesis of ZnO NSs, particularly ZnO NWs, via microwave-assisted ultrasonic technique, with the advantages of low cost and the potential for large scale. The samples were evaluated with respect to the structural, morphological, and optical properties using various methods, such as field-emission scanning electron microscopy, X-ray diffraction, and UV-Vis spectroscopy. The reaction occurs in only 60 minutes with minimal energy expenditure. ZnO NWs produced at 600 W had diameters ranging between 33.53 and 41.81 nm and lengths that varied between 1.84 and 2.1 µm, were totally crystalline, and showed preferential growth in the (002) direction, which presented a hexagonal wurtzite structure.

Article Info

https://doi.org/10.24191/mjcet.v6i2.21842

Article history:

Received date: 16 March 2023
Accepted date: 6 September 2023
Published date: 31 October 2023

Keywords:

Nanowires
Microwave
Ultrasonic
Deposition Time
Temperature

1.0 Introduction

Richard Feynman, a physicist, first identified the theoretical underpinnings of nanotechnology. A nanometer is one billionth of a meter, the most fundamental unit of measurement in use today. As important as they may be, nanotechnology requirements define how the prevailing specifications of current products will be incorporated into the development of future products (Shabannia & Hassan, 2013). Because of their potential utility in fields as diverse as optics, optoelectronics, catalysis, and piezoelectricity (Suzuki et al., 2019; Ghosh et al., 2004), research into and development of novel oxide-based multifunctional materials and one-dimensional nanostructures have expanded rapidly. In addition, zinc oxide (ZnO) is a nanostructured material that has been studied for decades because of its special characteristics, one of which improves electrical device performance (Guan et al., 2018; Meng et al., 2016). When compared to other semiconductors utilised in nanotechnology, its production costs are far cheaper, and its crystal-growth method is straightforward (Kubiak et al., 2021). ZnO has a significant excitation

binding energy (60 meV) at ambient temperature, with a band gap of 3.26 eV (Al-Gaashani et al., 2013; Wang et al., 2003). ZnO is a viable solution for electronics that need to function reliably at high temperatures. Wurtzite, which is hexagonal in shape (Toe et al., 2019), and zinc which is cubic, are the two most common ZnO crystal shapes (Ashok & Rao, 2017). ZnO nanowires (NWs) have attracted a lot of attention over the past decade due to their remarkable physical properties and potential applications in several emerging sectors, such as low-voltage and short-wavelength optoelectronics (Skoda et al., 2018), photonics (Chekroun et al., 2022), and solar cells (Zhang et al., 2014). Not only is it cheap, but it's also non-toxic, the fabric is stable, it's easily accessible, and it's highly transparent (Ravichandran et al., 2011). Recent evidence indicates that growth time can be reduced to minutes using microwave heating while still maintaining an appropriate film form and ZnO crystallinity. Conventional heating methods, on the other hand, can take up to 10 hours to reach the crystallisation temperature via convection, which can cause a thermal gradient throughout the bulk media and inefficient and non-uniform reactions, both of which can hinder crystal growth. Furthermore, microwave heating is a practical method for synthesising nanostructured materials due to its benefits, which include homogeneous volumetric heating, fast reaction rates, and energy savings (Rana , 2016). To speed up and improve the crystallisation process, microwave irradiation can be simply integrated into several synthesis procedures, like the thermal annealing approach. Microwave-assisted thermal annealing produces superior materials than those produced by conventional sintering methods.

2.0 Methodology

2.1 Material

Zinc Acetate Dihydrate [$Zn(CH_3CO_2)_2{\cdot}2H_2O$], Monoethanolamine, [MEA (C_2H_7NO)], 2-Methoxyethanol ($C_3H_8O_2$), Aluminium Nitrate Nonahydrate [$Al(NO_3)_3.9H_2O$], Zinc Nitrate Hexahydrate [$Zn(NO_3)_2.6H_2O$], HMTA [$C_6H_{12}N_4$], and DI water.

2.2 Preparing the seed layer

Zinc acetate dehydrate [$Zn(CH_3CO_2)_2{\cdot}2H_2O$] was dissolved in 2-methoxyethanol [$C_3H_8O_2$] at room temperature to create the precursor. The solution was then stabilised by the addition of monoethanolamine, [MEA (C_2H_7NO)]. Zinc acetate was present at a concentration of 0.4 mol/L, and the MEA:zinc acetate molar ratio was held constant at 1:1 (Malek et al., 2013). The solution was then doped with aluminium nitrate nonahydrate [$Al(NO_3)_3.9H_2O$] at a concentration of 1%.

Finally, the solution was agitated at 80 °C for 30 minutes on a hot plate stirrer to ensure that it was clear and uniform. The seed layer is typically prepared on a glass substrate. Acetone, methanol, and distilled water were used to ultrasonically clean the substrate for 10 minutes. The seed layer was applied to the substrate using spin-coating at 3000 rpm for 30 seconds after the solution was prepared. The sample was subsequently annealed in a furnace at 500 °C after being dried for 10 minutes at 300 °C on five separate occasions.

2.3 The growth of ZnO NWs on the seed layer

The second step, an aqueous solution of 12.5 mM zinc nitrate hexahydrate [$Zn(NO_3)_2.6H_2O$] and hexamethylenetetramine [HMTA, $C_6H_{12}N_4$] were used as a precursor, and stabiliser, respectively. To achieve a uniform solution, it was swirled in a beaker filled with distilled water for 30 minutes. The solution was then ultrasonically treated in a water bath at 50 °C for 30 minutes using a 40 kHz (Hwasin Technology Powersonic 405) and allowed to rest for 1 hour at room temperature to age. After that, the solution was stirred further for another 30 minutes without adding any heat. After that, the solution was transferred to a Scott bottle of 250 millilitres and the seed layer was submerged into the growing fluid. The Scott bottle then went into a 600-watt microwave for one hour.

Lastly, the sample was taken out from the growing solution and placed into a 500 °C annealing furnace. The sample growth was observed at five different period time (15, 30, 45, 60, and 75 minutes) to determine the impact of different time periods. The growth sample was analysed using X-ray diffraction (XRD, PANalytical X'Pert3 PRO), Field Emission Scanning Electron Microscope (FESEM, JEOL JSM-7600F) for morphological and microscopic analysis and UV-Vis-NIR spectrophotometer (Cary 5000) was used to analyse the transmittance of the sample.

3.0 Results and discussion

The structural and optical properties were studied to investigate the effect of growth time on the ZnO NWs.

3.1 The morphology and crystalline structure of the samples

The structural and crystal orientation features of ZnO NWs were significantly influenced by the duration they were allowed to grow. X-ray diffraction analysis was used to determine the crystal structure of the ZnO NWs. ZnO NWs with an average crystallite size of ~26.87 nm were formed at different stages during growth on a ZnO seed layer film, and their XRD patterns were displayed in Fig. 1. All samples show similar diffraction peaks with the hexagonal wurtzite structure of ZnO crystal (JCPDS No. 00-036-1451), with lattice parameters of a = 3.304 Å and c = 5.29 Å. According to the XRD patterns for all samples, the (100), (002), and (101) crystallographic planes of ZnO provide a dominant peak at 2θ ~ 31.36º, 33.88º, and 35.64º. The XRD patterns all share a prominent (002) orientation peak at 33.88º, which is the brightest of all the peaks. However, some orientation peaks show very low intensities, possibly due to the crooked arrangement of the ZnO NWs on the substrate.

The relative peak intensity $P_{(hkl)}$ of (002) orientation of the ZnO NWs was measured from its XRD pattern using the formula shown in Eq. (1).

$$P_{(hkl)} = \frac{I_{(hkl)}}{\Sigma I_{(hkl)}} \quad (1)$$

where $I_{(hkl)}$ is the *(hkl)* peak intensity and $\Sigma I_{(hkl)}$ is the sum of the intensities of all the diffraction peaks of the ZnO NWs. The relative peak intensity of the (002) plane for ZnO NWs is shown in Table 1. A significant increase in the intensity ratio of the (002) peak, I (002) / ΣI (hkl), indicates that the material preferentially grows along the c-axis crystallographic plane, which introduces the least surface energy. The relative peak intensity of ZnO NWs grown for 60 minutes is 0.763, which is substantially higher than that of ZnO NWs grown for 30 minutes P (002) = 0.433. The average crystallite size, D of the ZnO NWs deposited at various growth time was obtained by Scherrer's formula shown in Eq. (2).

$$D_{(hkl)} = \frac{k\lambda}{\beta_{(hkl)} \cos\theta} \quad (2)$$

where k is the correction factor (0.94), λ is the X-ray wavelength (1.54 Å), β is the full width at half maximum of the (002) plane wavelength in radians and θ is Bragg's angle in degrees. The average crystallite size of ZnO NWs decreases from 15 to 45 minutes as the growth duration increases. However, the sample with a growth time of 60 minutes has the highest relative peak intensity, crystallite size, and FWHM value. This observation indicated that their crystal quality improved as the growth time of ZnO NWs increased. The diffractive angle, relative peak intensity relative to the ZnO (002) plane, FWHM, and average crystallite size of the aligned ZnO NWs were summarised in Table 1.

Images of the surface morphology of thin films containing an array of ZnO NWs, obtained at 50 k magnification and at varying intervals during growth, are displayed in Fig. 2. The growth duration ranged from 15 minutes to 75 minutes in this experiment. The images show that uniform and dense ZnO NWs structures were deposited on the substrates, and that they are big and well-oriented. The ZnO NWs have a flat top and a hexagonal structure. Growing the structure from 15 to 75 minutes results in a homogeneous hexagonal shape. The homogeneity of the ZnO NWs formed on this seed layer is remarkable.

Table 1: Diffraction angle, relative peak intensity, FWHM, and crystallite size at various growth time

Growth Time (min)	Diffraction angle, 2θ(°)	Relative Peak Intensity (002)	FWHM (degree)	Crystallite size, D (nm)
15	33.89	0.609	0.339	25.60
30	33.82	0.433	0.353	24.52
45	33.86	0.449	0.356	24.32
60	33.88	0.763	0.323	26.87
75	33.89	0.565	0.347	24.96

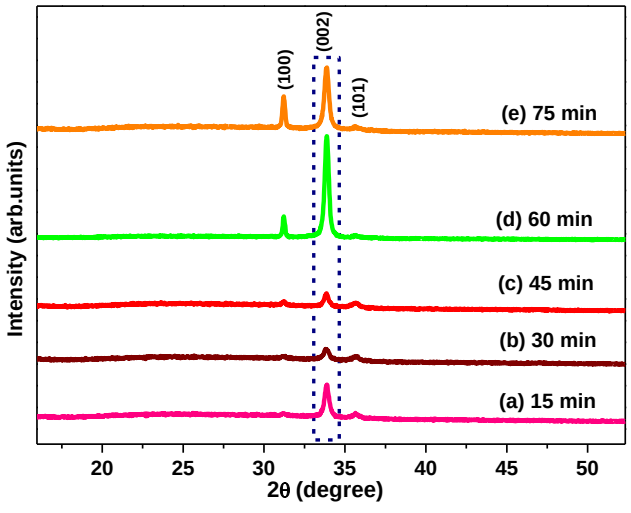

Fig. 1: The XRD patterns of ZnO NWs prepared at various growth time

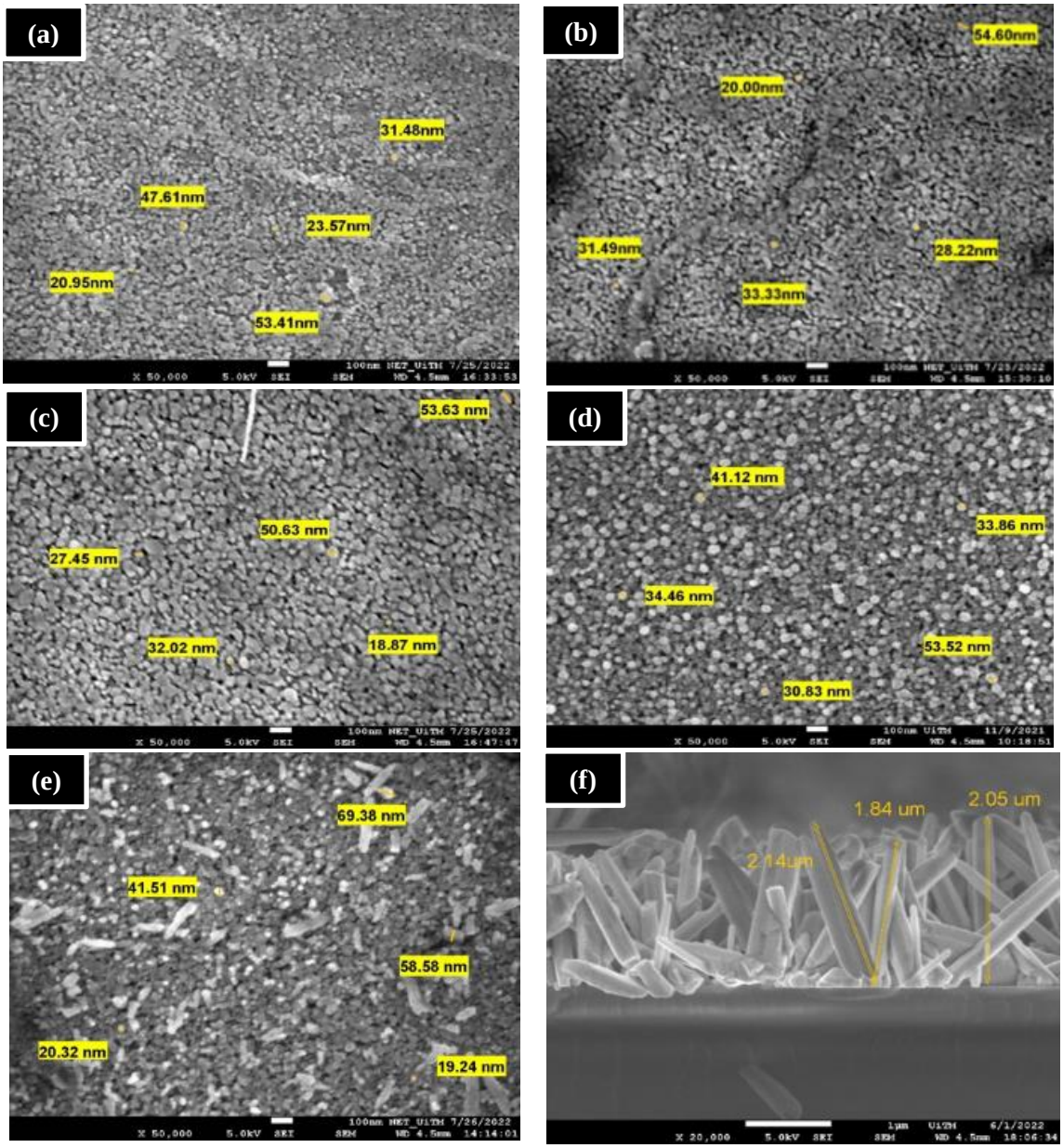

Fig. 2 : FESEM morphology of ZnO NWs of (a) 15, (b) 30, (c) 45, (d) 60, (e) 75 min [5 kV applied voltage; 50 K magnification] and (f) Average thickness of the films [5 kV applied voltage; 20 K magnification]

Similar trends may be seen in the morphology of ZnO NWs as a function of development time; this may be attributable to hydrothermal processes being accelerated when they occur over a seed surface free of blanks and lumps, which can impede growth. Fig. 2 (a) displays the surface morphology of ZnO NWs deposited for 15 minutes, which reveals aggregated hexagonal grains and a more compact structure than other samples. Furthermore, nucleation and crystallisation growth process initiate the expansion of aligned ZnO NWs (Guan et al., 2018). During the initial nucleation stage, the temperature of the reaction system rises quickly and exceeds the boiling point of water in 10 minutes. The milky white solution demonstrates the production of many identical ZnO nuclei during condensation and hydrolysis. Due to differences in the surface energy of crystallographic planes, the ZnO nuclei developed into NWs.

These outcomes are the end consequence of the growth-related Ostwald ripening process. Ostwald ripening causes the formation of crystals or particles to change densities over time. This phenomenon represents the gradual change in the structure of a homogeneous system over time, and it occurs in both solid and liquid solutions. There are several possible time reactions for this procedure. The diameter of ZnO NWs increased as the time increased from 15 to 75 minutes, confirming the transverse and longitudinal growth of NWs with time. This change can be due to the anisotropy of the ZnO material. Crystal planes with a higher surface energy grow at a quicker rate. As a result of their different surface energies, (002) planes

develop more quickly than others. Since the development rates of the multiple crystal planes are not the same, the surfaces with quicker growth velocities will lose area first, while the surfaces with slower growth velocities will eventually dominate the crystal's morphology. As a result, a 1-D structure forms with a breadth that varies throughout its length. The longer the reaction period, the more of the zinc species in the solution can be consumed. Thermodynamics will govern the reaction process and the Ostwald ripening will be observable in this case (Guan et al., 2018). Fig. 2 and Table 2 show that when the growth period increases, there is only a minor rise in the average diameters of the NWs across all samples, ranging from 33.53 to 41.81 nm, while the shape remains the same. However, these NWs are nearly identical in diameter across the board. Conclusion can be drawn that despite the prolonged period of growth, there was no change in diameter. NWs lengths were determined by performing cross-sectional scanning electron microscopy on the substrates. It was calculated that 2.01 μm of growth occurs in just 60 minutes. Furthermore, this indicates that, under the conditions of our experiment, axial growth reaches a plateau, whereas radial growth continues to expand. It would be interesting to investigate the correlation between the axial and radial growth modes of ZnO NWs and other factors, such as the pH, composition, and concentration of the precursor solution and the diffusion dynamics on the ZnO NWs' surfaces. Different zinc oxide morphologies result from changes in crystal growth rates associated with different crystallographic planes (Yuliasari et al., 2022). The average diameter of aligned ZnO NWs developed over different times were summarised in Table 2.

3.2 The optical properties of the samples

The optical properties of ZnO NWs were determined using UV-Vis-NIR spectrophotometer measurements between 350 and 800 nm at room temperature. UV-Vis transmittance spectrum analysis of ZnO NWs of different growth times was performed as shown in Fig. 3. In all cases, the films were transparent, which is defined as above 80% in the visible range. The absorption edges lie below 400 nanometres. Particle size difference has been extensively stated to be the origin of the observed variance in the absorption edges (Mamat et al., 2014). The longer the wires are exposed to radiation, the larger they grow radially (in a process known as Ostwald ripening), which could be another factor in the change in transmittance. Microwave irradiation is thought to interact with ZnO growth units to produce active centres on the surface of ZnO nuclei, allowing the formation of ZnO NWs with varying energy gaps (Yadav et al., 2008). The random distribution of the ZnO NWs in the film and the resulting internal tension may also be to blame for this motion (Hayamizu et al., 1996). As growth durations increase, the transmittance is hindered by the modest dependence of film thicknesses on growth time.

Samples grown in 15 minutes showed the highest transmittance, with an average transmittance of 90.74% between 400 and 800 nm in the visible region, while samples immersed for 75 minutes showed the lowest transmittance, with an average transmittance of 82.51% over the same wavelength range. Table 3 provides all available information about average transmittance. Using the Lorentz-Lorentz relation in equation Eq. (3), researchers examined how to estimate the ZnO NWs structure's porosity written as Gupta (1996).

$$Porosity = 1 - \left[\frac{\left[\left(n_f^2-1\right)/\left(n_f^2+2\right)\right]}{\left[\left(n_s^2-1\right)/\left(n_s^2+2\right)\right]}\right] \qquad (3)$$

where n_f is the refractive index of the porous ZnO films and ns is the refractive index of the ZnO skeleton, which is widely accepted as 2. The index of refraction, n_f at different wavelengths was calculated using the envelope curve for transmittance maxima (T_{max}) and transmittance minima (T_{min}) in the transmission spectra.

Table 2 : Average diameter ZnO NWs at various growth time

Growth Time (min)	Average Diameter (nm)
15	33.53
30	35.40
45	36.52
60	38.76
75	41.81

Table 3: Average transmittance, refractive index and porosity of ZnO NWs at various growth time

Growth Time (min)	Average Transmittance (%)	Refractive index, n_f	Porosity (%)
15	90.74	1.564	34.98
30	88.83	1.633	28.53
45	88.14	1.657	26.41
60	87.81	1.668	25.43
75	82.51	1.837	11.66

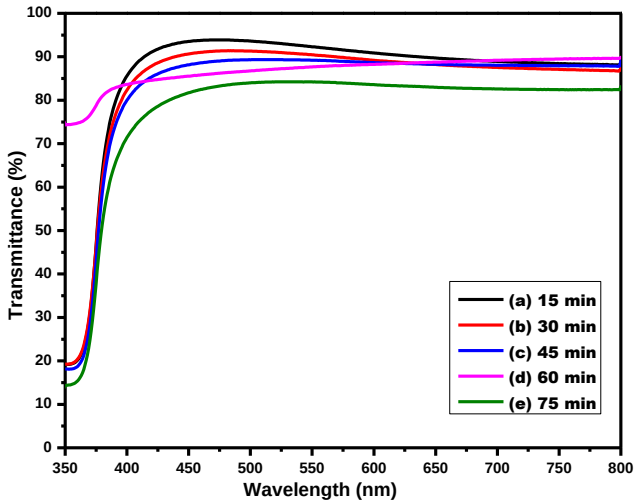

Fig. 3: Transmittance spectra of ZnO NWs prepared at various growth time

The expression for refractive index is given by the following expressions [Eq. (4) and Eq. (5)].

$$n_f = \left[N + (N^2 - s^2)^{1/2}\right]^{1/2} \quad (4)$$

$$N = \frac{2s}{T_m} - \left(\frac{(s^2+1)}{2}\right) \quad (5)$$

where T_m is the envelope function of the T_{max} and T_{min} while s is the refractive index of the substrate.

The T_m value is obtained by taking the average of the transmittance data from the transparent region, or the region where the α value is close to 0 which is between the wavelength of 400 and 800 nm.

The measured porosity values were 34.98% at 15 minutes, 28.53% at 30 minutes, 26.41% at 45 minutes, 25.43% at 60 minutes, and 11.66% at 75 minutes of growth. Since transmittance values decreased as growing time rose, the refractive index, n_f, increased from 1.564 to 1.837. The creation of micropores and nanopores in the ZnO crystallite structure is frequent for samples made using a solution-based approach, and this may account for the observed result of increased thickness. In addition, the chart shows that the ZnO NWs structure loses porosity as growth time increases. All of the ZnO NWs have had their computed porosity and refractive index, n_f, summarised in Table 3.

4.0 Conclusions

ZnO NWs have been successfully synthesised using microwave-assisted ultrasonic techniques. The XRD pattern revealed a highly crystalline phase of the material with an average crystallite size of 25.25 nm. ZnO NWs grown at 600 W had diameters of 33.53 – 41.81 nm and lengths of 1.84 – 2.1 nm; they were fully crystalline, grew preferentially in the (002) direction, and displayed a hexagonal wurtzite structure. With an absorption of less than 15%, these crystalline films were transparent. These findings should promote the practical application of crystalline ZnO films, such as large-area transparent electrodes. Future applications of ZnO should take advantage of its distinctive properties to facilitate the development of new application fields.

Contribution statement

Mohd Firdaus Malek, Mohamad Hafiz Mamat & Mohamad Rusop Mahmood: Conceptualisation and supervision; **Nurul Zulaikha Mohd Zamri, Mohd Firdaus Malek & Maryam Mohammad:** Methodology; **Nurul Zulaikha Mohd Zamri, Maryam Mohammad, Mohd Dzulfiqar Bakri, Nur Fairuz Rostan & Nurfatini Atiqrah Khairul Azhar:** Formal analysis and investigation; **Mohd Firdaus Malek, Mohamad Hafiz Mamat & Muhammad Salleh Shamsudin:** Resources; **Nurul Zulaikha Mohd Zamri, Mohd Dzulfiqar Bakri, Nur Fairuz Rostan & Nurfatini Atiqrah Khairul Azhar:** Writing-original draft; **Mohd Firdaus Malek, Nur Fairuz Rostan & Muhammad Salleh Shamsudin:** Writing-review and editing; **Mohd Firdaus Malek & Mohamad Rusop Mahmood:** Project administration.

Conflict of Interest

The authors declare that they have no known competing financial interests or personal relationships that could have appeared to influence the work reported in this paper.

Acknowledgement

This work was supported by Grant Nos. 600-RMC/YTR/5/3 (005/2021) and 600-RMC/GIP 5/3 (098/2021) under Universiti Teknologi MARA (UiTM), Malaysia. The authors would like to thank the Research Management Centre (RMC), Universiti Teknologi MARA (UiTM), Malaysia, for their support.

References

Al-Gaashani, R., Radiman, S., Daud, A.R., Tabet, N., & Al-Douri, Y. (2013). XPS and optical studies of different morphologies of ZnO nanostructures prepared by microwave methods. *Ceramics International, 39*, 2283–2292. https://doi.org/10.1016/j.ceramint.2012.08.075

Ashok C.H., & Rao, K. V. (2017). Synthesis of nanostructured metal oxide by microwave-assisted method and its humidity sensor application. *Materials Today Proceedings*, *4*(2) Part A, 3816–3824. https://doi.org/10.1016/j.matpr.2017.02.279

Chekroun, M.Z., Benali, M.A., Yahiaoui, I.E., Debab, M., Belmehdi, M. Z., & Tabet-Derraz, H. (2022). Optical properties behavior of ZnO nanoparticles deposited on glass in the ultraviolet–visible spectral range: Experimental and numerical study. *Optical Materials, 132*, 112769. https://doi.org/10.1016/j.optmat.2022.112769

Ghosh, R., Basak, D., & Fujihara, S. (2004). Effect of substrate-induced strain on the structural, electrical, and optical properties of polycrystalline ZnO thin films. *Journal of Applied Physics, 96*, 2689–2692. https://doi.org/10.1063/1.1769598

Guan, X., Li, L., Liu, J., & Li, S. (2018). Effects of ultrasonic-microwave-assisted technology on hordein extraction from barley and optimization of process parameters using response surface methodology. *Journal of Food Quality, 2018*, 9280241. https://doi.org/10.1155/2018/9280241

Gupta, V., & Mansingh, A. (1996). Influence of postdeposition annealing on the structural and optical properties of sputtered zinc oxide film. *Journal of Applied Physics*. *80*(2), 1063–1073. https://doi.org/10.1063/1.362842

Hayamizu, S., Tabata, H., Tanaka, H., & Kawai, T. (1996). Preparation of crystallized zinc oxide films on amorphous glass substrates by pulsed laser deposition, *Journal Applied Physics, 80*(3), 787–791. https://doi.org/10.1063/1.362887

Kubiak, A., Sonia, Ż., & Siwi, K. (2021). Controlled microwave-assisted and pH-affected growth of ZnO structures and their photocatalytic performance. *Powder Technology, 386*, 221–235. https://doi.org/10.1016/j.powtec.2021.03.051

Malek, M.F., Mamat, M.H., Sahdan, M.Z., Zahidi, M.M., Khusaimi, Z., & Mahmood, M.R. (2013). Influence of various sol concentrations on stress/strain and properties of ZnO thin films synthesised by sol–gel technique. *Thin Solid Films, 527*, 102–109. https://doi.org/10.1016/j.tsf.2012.11.095

Mamat, M.H., Malek, M.F., Hafizah, N.N., Khusaimi, Z., Musa, M. Z., & Rusop, M. (2014). Fabrication of an ultraviolet photoconductive sensor using novel nanostructured, nanohole-enhanced, aligned aluminium-doped zinc oxide nanorod arrays at low immersion times. *Sensors and Actuators B: Chemical, 195*, 609–622. https://doi.org/10.1016/j.snb.2014.01.082

Meng, L. Y., Wang, B., Ma, M. G., & Lin, K. L. (2016). The progress of microwave-assisted hydrothermal method in the synthesis of functional nanomaterials, *Materials Today Chemistry, 1–2* 63–83. https://doi.org/10.1016/j.mtchem.2016.11.003

Rana, A., Kang, M., & Kim, H. (2016). Microwave-assisted facile and ultrafast growth of ZnO nanostructures and proposition of alternative microwave-assisted methods to address growth stoppage. *Scientific Reports, 6*, 24870. https://doi.org/10.1038/srep24870

Ravichandran, C., Srinivasan, G., Lennon, Sivananthan, S., & Kumar, J. (2011). Influence of post-deposition annealing on the structural, optical and electrical properties of Li and Mg co-doped ZnO thin films deposited by sol-gel technique. *Superlattices and Microstructures, 49*(5), 527–536. https://doi.org/10.1016/j.spmi.2011.03.005

Shabannia, R., & Hassan, H.A. (2013). Growth and characterization of vertically aligned ZnO nanorods grown on porous silicon: Effect of precursor concentration. *Superlattices and Microstructures. 62*, 242–250. https://doi.org/10.1016/j.spmi.2013.07.025

Skoda, D., Urbanek, P., Sevcik, J., Munster, L., Antos, J., & Kuritka, I. (2018). Microwave-assisted synthesis of colloidal ZnO nanocrystals and their utilization in improving polymer light emitting diodes efficiency. *Materials Science Engineering: B, 232-235*, 22–32. https://doi.org/10.1016/j.mseb.2018.10.013

Suzuki, V.Y., de Paula, N.H., Gonçalves, R., Li, M.S., Pereira, E.C., Longo, E., & La Porta, F.A. (2019). Exploring effects of microwave-assisted thermal annealing on optical properties of Zn2GeO4 nanostructured films. *Materials Science and Engineering: B, 246*, 7–12. https://doi.org/10.1016/j.mseb.2019.05.023

Toe, M.Z., Jusoh, N.A.H.N., Pung, S.Y., Yaacob, K.A., Matsuda, A., Tan, W.K., & Han, S.S. (2019). Effect of ZnO seed layer on the growth of ZnO nanorods on silicon substrate. *Materials Today Proceedings, 17*(3), 553–559. https://doi.org/10.1016/j.matpr.2019.06.334

Wang, Y.G., Lau, S. P., Lee, H. W., Yu, S. F., Tay, B. K., Zhang, X. H., Tse, K. Y., & Hng, H. H. (2003). Comprehensive study of ZnO films prepared by filtered cathodic vacuum arc at room temperature. *Journal of Applied Physics, 94*(3), 1597–1604. https://doi.org/10.1063/1.1592007

Yadav, R.S., Mishra, P., & Pandey, A.C. (2008). Growth mechanism and optical property of ZnO nanoparticles synthesized by sonochemical method. *Ultrasonics Sonochemistry, 15*(5). 863–868. https://doi.org/10.1016/j.ultsonch.2007.11.003

Yuliasari, F., Aprilia, A., & Hidayat, R. (2022). Improved dye-sensitized solar cell performance with hedgehog-like shaped ZnO nanorods grown using ZnO nanoparticles seed layer. *Mateials. Today Proceedings, 52*(2), 248–251. https://doi.org/10.1016/j.matpr.2022.02.193

Zhang, M., Zhang, M., Shi, S., Song, X., & Sun, Z. (2014). An approach toward TiO2 nanostructure growth with tunable properties: Influence of reaction time in a hydrothermal process. *Journal of Alloys and Compounds, 591*, 213–217. https://doi.org/10.1016/j.jallcom.2013.12.227